J. Biochem. **141,** 459–468 (2007)
doi:10.1093/jb/mvm051

Determination of the Role of the Carboxyl-terminal Leucine-122 in FMN-binding Protein by Mutational and Structural Analysis

Masaya Kitamura[1,*,†], Koji Terakawa[1], Hideo Inoue[1], Takuto Hayashida[2], Kyoko Suto[2], Yukio Morimoto[2,3], Noritake Yasuoka[2], Naoki Shibata[2,3] and Yoshiki Higuchi[2,3,†]

[1]Department of Applied and Bioapplied Chemistry, Graduate School of Engineering, Osaka City University, 3-3-138 Sugimoto, Sumiyoshi-ku, Osaka 558-8585; [2]Graduate School of Life Science, University of Hyogo, 3-2-1 Kouto, Kamigori Ako-gun, Hyogo 678-1297; and [3]RIKEN Harima Institute/SPring-8, 1-1-1 Koto, Mikazuki-cho, Sayo-gun, Hyogo 679-5248, Japan

Received December 25, 2006; accepted January 3, 2007; published online January 29, 2007

Mutants of flavin mononucleotide-binding protein (FMN-bp) were made by site-directed mutagenesis to investigate the role of carboxyl-terminal Leu122 of the pairing subunit in controlling redox potentials, binding the prosthetic group, and forming the tertiary and quaternary structure. We compared the oxidation–reduction potentials, FMN-binding properties, and higher structures of wild-type FMN-bp and four mutant proteins (L122Y, L122E, L122K and L122-deleted). We found that the redox potentials were affected by mutations. Also, the affinities of L122E, L122K and L122 deletion mutant apoproteins for FMN were lower than for the wild-type apoprotein, whereas the affinity of L122Y for FMN was increased. Analytical ultracentrifugation showed that the dissociation constants for dimerization of L122E and L122K were larger than for wild-type FMN-bp, whereas the dissociation constants for L122Y and the deletion mutant were lower than for the wild type. Finally, we determined the higher structures of L122Y, L122E and L122K mutants by X-ray crystallography. Our results show that the mutation of Leu122 in FMN-bp changes midpoint potentials, dissociation constants for FMN, and dimer formation, indicating that this residue is important in the pairing subunit.

Key words: crystal structure, dimer formation, dissociation constant, FMN-binding protein, redox potential.

Abbreviations: *D.*, *Desulfovibrio*; FMN-bp, FMN-binding protein; NCS, non-crystallographic symmetry; PNPOx, pyridoxine 5′-phosphate oxidase.

After Ulmer elucidated the importance of studying protein engineering about 20 years ago (*1*), many studies using mutagenesis techniques have explained the relationship between the structure and function of the protein. In his prospects for protein engineering, 'cofactor requirement' was one of the important properties to control activities. In redox proteins that have some cofactor, that is, hemes, iron–sulphur clusters, flavin derivatives and so on, the peptide portion is thought to play a role not only as a 'frame' for the cofactor but also to choose the correct partner for the redox reaction, to determine its redox potential, and to bind the cofactor as tightly as needed. To carry out their biological functions, sulphate-reducing bacteria have many redox proteins, which contain various tightly bound cofactors (*2*). At least five types of flavoprotein that non-covalently bind FMN have been identified in *Desulfovibrio* (*D.*), but they have different structures (*3–7*). In flavin derivatives, redox reactions are confined to the isoalloxazine ring, and the rest of the molecule is thought to be important for binding and controlling redox potential. On binding to the protein, the redox properties of the flavin are tailored to suit the particular requirements of the redox reaction in which the protein is involved (*8*).

FMN-binding protein (FMN-bp) is one of the smallest flavoproteins identified to date. It is composed of 122 amino-acid residues and one molecule of FMN but lacks cysteine residues. Using genetic engineering methods, it has been expressed in *Escherichia coli* and purified (*4*). Within each bacterial strain, the redox properties and amino-acid sequences of FMN-bps differ from those of flavodoxin (*3*). The solution structure of FMN-bp has been solved by NMR spectroscopy, and it has been shown to be similar to the hypothetical single-domain precursor of chymotrypsin (*9*); however, Murzin (*10*) pointed out the structural similarity between FMN-bp and ferredoxin reductase superfamily of flavoenzymes. Indeed, the FMN-binding domains from phthalate dioxygenase reductase and FMN-bp are homologous, but none of the FMN-binding domains yielded a low root mean square deviation when the alpha carbons were aligned with the carboxyl-terminal domain of the hepatitis virus 3C protease (*11*). A recent crystal structure of FMN-bp

*To whom correspondence should be addressed
Tel: +81-6-6605-3091, Fax: +81-6-6605-2782,
E-mail: kitamura@bioa.eng.osaka-cu.ac.jp
†The first and last authors contributed equally to the work.

revealed a dimeric form (*12*). The molecular interfaces between monomers were flat and hydrophobic in the central part, and there were also hydrophilic interactions surrounding them. The cofactor FMN was situated in the groove near the interface and held in place by hydrophobic and hydrophilic interactions. It was also suggested that the carboxyl-terminal residue Leu122 in the pairing molecule, which forms a hydrophobic core with Trp32 and Val115, has an important role in the interaction with the *o*-xylene moiety in FMN (*13*).

The determinants of redox potential and the mechanism by which the FMN cofactor binds to apoflavoprotein are subject of some debate. Flavodoxin is the most well-studied flavoprotein. Although the crystal and NMR structures of many flavodoxins and flavodoxin mutants have been solved (*14*, *15*), there are still many questions to be answered, for example, how the initial interaction between FMN and apoflavodoxin, and the resulting conformational change of apoflavodoxin affect the binding of FMN. Recently, stopped-flow kinetic analysis of FMN binding by *D. vulgaris* flavodoxin has shown that it is influenced by inorganic phosphate (*16*); however, the K_d for FMN and apoflavodoxin estimated by this method was ~10-fold higher than that reported by Curley *et al*. (*17*). The mechanism of FMN binding to *D. vulgaris* flavodoxin was also confirmed by near-UV circular dichroism, intrinsic fluorescence spectroscopy and NMR analysis of holoflavodoxin, riboflavin-flavodoxin complex and apoflavodoxin (*18*). Based on these studies, they proposed a model for the binding of FMN to apoflavodoxin in which inorganic phosphate is bound in the ring-first binding mode, and in the phosphate-first binding mode the phosphate moiety triggers a change in the flavin-binding subsite that promotes ring binding. On the other hand, the electrostatic effects of Glu or Asp residues near FMN on redox potentials of the flavodoxin and the redox potential between semiquinone and hydroquinone have been reported to correlate with the number of acid-to-amide substitutions (*19*). However, we have found that the relationship between the number of acidic amino-acid residues and the redox properties may be complex (*3*). It was also reported that the redox potentials were modulated by hydrogen bonding interactions between the N(3)H of FMN and Glu59 in *Clostridium* flavodoxin or between N(1) of FMN and Asp95 in *D. vulgaris* flavodoxin (*20*, *21*). Although FMN-bp and flavodoxin have almost the same molecular weight and both bind to FMN from the same strain of *D. vulgaris*, they have different amino-acid sequences, FMN-binding region structures and higher structures. Therefore, the mechanisms by which FMN binds to the apoflavoprotein may differ. For this reason it is important to clarify the effect of the FMN-binding mode and dimer formation on the redox properties of FMN-bp.

In the present article, we report on the mutational analysis of Leu122 residue in FMN-bp from *D. vulgaris* (Miyazaki F). We also discuss the relationship between redox potentials and the molecular environment around FMN, the binding of FMN and the higher structure of FMN-bp.

EXPERIMENTAL PROCEDURES

Site-directed Mutagenesis—The gene for FMN-bp is contained in the 419-bp *Eco*RI-*Hin*dIII insert of pBT-100 (*4*). Site-directed mutagenesis was carried out using a modification of the method of Inoue (*22*) and using the following oligonucleotides: L122Y, 5′-GAGCAGACCTACTAGGCGGGC-3′; L122E, 5′-GAGC AGACCGAGTAGGCGGG-3′; L122K, 5′-GAGCAGACCAA GTAGGCGGG-3′ and L122-deleted (L122del), 5′-GAGC AGACCTAGTAGGCGGG-3′. Dideoxy nucleotide sequencing was used to confirm the presence of the mutation. The mutated *Eco*RI-*Hin*dIII fragment was ligated into the pMK2 expression vector, and *Escherichia coli* (JM109) cells were transformed with these plasmids.

Expression and Purification of FMN-bp Mutants—Wild-type and mutant FMN-bps were purified essentially in the holo form (FMN-bound) as described previously (*4*). ApoFMN-bps were subsequently prepared by treatment with 0.1% trichloroacetic acid, followed by purification by reversed-phase HPLC using a Nucleosil C8 column (0.46×25 cm) with a linear gradient of acetonitrile in 0.1% trifluoroacetic acid at a flow rate of 0.8 ml/min. The fractions were collected, dialyzed against water overnight, and lyophilized. Each apoFMN-bp was confirmed to be >95% pure by SDS-polyacrylamide gel electrophoresis (*23*).

Midpoint Potential Determinations—The midpoint potentials of the wild-type and mutant FMN-bps were determined spectrophotometrically at 25°C by equilibration in 200 mM potassium phosphate (pH 7.0) with the standard redox dye safranine T ($E_{m,7} = -289$ mV) (*24*). Protein and dye solutions were made anaerobic by subjecting them to several cycles of vacuum and flushing with argon gas in a closed-cuvette apparatus. UV-visible absorption spectra were recorded on a Hitachi U-3000IR spectrophotometer during reductive titration with sodium dithionite until equilibrium was reached between all species in solution. The midpoint potentials were determined as the point at which the concentrations of oxidized and reduced dye were equal, using the following relationship:

$$E_{\mathrm{FMN-bp}} - E_{\mathrm{dye}} = \frac{RT}{nF} \ln \frac{[\mathrm{FMN-bp}]_{\mathrm{ox}}}{[\mathrm{FMN-bp}]_{\mathrm{red}}}$$

where $E_{\mathrm{FMN\text{-}bp}}$ is the midpoint potential of wild-type and mutant FMN-bps, E_{dye} is the midpoint potential of the redox indicator dye, $[\mathrm{FMN\text{-}bp}]_{\mathrm{ox}}$ is the concentration of oxidized FMN-bp, $[\mathrm{FMN\text{-}bp}]_{\mathrm{red}}$ is the concentration of reduced FMN-bp, R is the gas constant, T is the temperature in degrees Kelvin, F is the Faraday constant and n is the number of electrons involved in the reduction (two in this case). The midpoint potentials calculated by linear regression analysis of the plots of the system potential determined by the absorbance of dye at 517 nm, where the absorbance of FMN-bp is zero, versus the logarithm of the ratio of concentrations of the oxidized and reduced forms of the FMN-bp determined by the absorbance at 408 nm, where is located the isosbestic point of safranine T. Absorbance was corrected for dilution caused by the addition of sodium dithionite solution.

The data are reported relative to the potential of the standard hydrogen electrode.

Dissociation Constants—FMN can be removed from the protein to form apoFMN-bp, which can then be easily reconstituted to FMN-bp by the addition of FMN. The dissociation constants of the complexes between FMN and apoFMN-bp were determined in the dark at $25 \pm 0.1^{\circ}C$ by titrating with apoFMN-bp and following the quenching of FMN fluorescence. In a typical experiment, 3 ml of 0.1 μM FMN in 50 mM potassium phosphate buffer (pH 7.0) and 5 mM EDTA were titrated with aliquots of 4 to 15 μM apoFMN-bp. Quenching of FMN fluorescence occurred within several minutes. The emission value at 524.8 nm was recorded, and the proportion of bound FMN was determined at equilibrium by measuring the extent of quenching. Fluorescence values were corrected according to the dilution caused by the addition of apoFMN-bp solution. The dissociation constants (K_d) were then calculated as described previously (*5*). The midpoint potentials of ApoFMN-bp:FMN complexes are linked to the binding affinities of different FMN at the redox states by the thermodynamic cycle shown in Fig. 1, allowing the K_d values for hydroquinone complexes to be calculated. Thus, free energy for the ApoFMN-bp:FMN_{ox} complex (ΔG_{ox}) can be obtained directly from K_d values, while those of the ApoFMN-bp:FMN_{red} complex (ΔG_{red}) can be calculated from the following equation:

$$\Delta G_{red} = \Delta G_{ox} - 2F\left(E_{FMN-bp} - E_{free\ FMN}\right)$$

where F is also Faraday's constant and the midpoint potential of free FMN ($E_{free\ FMN}$) is −221 mV (25°C, pH 7) considering ionic strength (*25*). Then the dissociation constants for hydroquinone were calculated from the following equation:

$$K_d^{reduced\ FMN} = \exp(-\Delta G_{red}/RT)$$

where R is the gas constant ($8.31\ J\ K^{-1}\ mol^{-1}$) and T is temperature (298 K).

Analytical Ultracentrifugation—Sedimentation velocity experiments were carried out with holoFMN-bp at 20.0°C using a Beckman XL-I analytical ultracentrifuge with absorbance optics and following the procedure described by Laue and Stafford (*26*). Protein solutions were exhaustively dialysed against 20 mM Tris–HCl (pH 8.0) containing 200 mM NaCl. Experiments were performed at 26,127*g* for ~20 h, and absorbance was measured at 280 and 439 nm. The concentrations of wild-type and mutant FMN-bps were 0.39 to 0.55 mg/ml. K_D was calculated using the program EQASSOC using a partial specific volume of the monomer = 0.738 (L122Y and L122E mutants) or 0.739 (wild-type and L122K and L122del mutants).

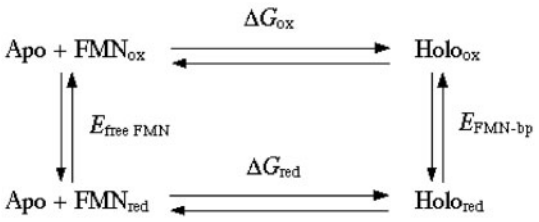

Fig. 1. **Thermodynamic cycle showing the relationship between the midpoint potentials and bound FMN with the affinity constants of the oxidized and hydroquinone ApoFMN-bp:FMN complexes.**

Crystallization and Data Collection—Single crystals for the three mutant proteins were grown from concentrated (15 mg/ml) protein solutions using the hanging drop vapour diffusion method with a seeding technique (*12*). For the L122Y and L122K mutants, 8 μl of protein solution was mixed with the same volume of outer precipitating solution (0.1 M Tris–HCl (pH 7.5) containing 20% (w/v) polyethylene glycol 6000, 0.2 M sodium acetate and 20% glycerol). For the L122E mutant, 0.1 M Tris–HCl (pH 7.5), 20% (w/v) polyethylene glycol 6000, 0.2 M sodium acetate and 20% 2-methyl-2,4-pentandiol were used as the outer precipitating solution. Diffraction intensity data for the mutant crystals were collected using an X-ray beam from synchrotron radiation at beamlines BL-40B2 (ADSC Quantum 4R CCD detector) and BL-44XU (Oxford CCD detector) at SPring-8, Japan (Table 1). The program *HKL2000* was used for data processing (*27*).

Refinement—The initial phases for the three mutants were obtained by a conventional molecular replacement method using the *ARP/wARP* package (*28*) with coordinates for wild-type FMN-bp (PDB code 1flm) as the starting model. A whole molecular model of each mutant was built into the map and improved with successive solvent flattening, histogram mapping and non-crystallographic symmetry (NCS) averaging based on the matrix calculated from the partial model. The structures were refined using the program *CNS* (*29*). In the initial stage of refinement for the L122E mutant, NCS restraints were introduced because two dimers were closely packed into the asymmetric unit. After the structure was well refined (R-factor <0.25), NCS restraints were removed, and final refinement cycles were carried out. The model for L122Y was refined using *SHELXL* (*30*) after refinement with *CNS* because the side chain of the carboxyl terminal L122Y residue showed double conformers.

Table 1. **Data collection.**

Data collection	L122Y	L122E	L122K
Space group	$P2_1$	$P2_1$	$P2_1$
Unit cell			
a (Å)	36.67	60.16	36.72
b (Å)	79.39	57.96	83.32
c (Å)	39.97	62.02	40.41
β(°)	91.25	91.54	93.86
No. of molecules in a.u.	4	8	4
Resolution (Å)	30.0–1.60	30.0–1.90	30.0–1.60
(Outer shell)[a]	(1.66–1.60)	(1.97–1.90)	(1.66–1.60)
Total reflections	109,713	127,555	113,803
Unique reflections[a]	29,692 (2543)	33,783 (3310)	30,132 (2097)
Completeness (%)[a]	98.0 (84.7)	99.5 (98.6)	93.7 (66.0)
R_{merge} (%)[a]	3.2 (6.2)	7.7 (20.6)	2.8 (8.9)
$\langle I \rangle / \langle \sigma(I) \rangle$[a]	43.4 (22.9)	15.2 (3.4)	40.6 (16.7)
Redundancy	3.7	3.7	3.8

[a]Values in outer shell are in parentheses.

RESULTS

Midpoint Potentials of Wild-type and Mutant FMN-bps—Binding of ApoFMN-bp to FMN modifies the free FMN midpoint potential by being displaced to a negative value. In the current studies, we showed that FMN is situated in the groove near the dimer interface of FMN-bp and held in place by hydrophobic and hydrophilic interactions. In addition, we showed that the carboxyl terminal leucine in the pairing molecule plays an important role in the interaction with the *o*-xylene moiety of FMN (*13*). The midpoint potential of flavodoxin from *D. vulgaris* (Hildenborough) is thought to be controlled by the electrostatic environment of the FMN-binding site (*8*). We therefore examined the effect of mutating the Leu122 residue to Glu or Lys. These mutations were also intended to change the hydrophobicities around FMN. It was expected that a L122Y mutant would have enhanced FMN and monomer binding, and that this might alter the redox properties of FMN-bp. We also sought to directly examine the role of Leu122 by deleting it.

As the semiquinone state of FMN-bp may not be entirely stable, it is possible that its spectrum could be detected through careful reduction. Therefore, oxidation–reduction potentials for the fully oxidized state/fully reduced state couple of the FMN cofactor bound to FMN-bps were established by equilibration with appropriate redox indicator dyes and fitting of the data to the Nerst equation, as shown in Fig. 2. The slope of the lines for the wild-type and mutant FMN-bps was 1.0. The midpoint potentials for each FMN-bp are shown in Table 2. We previously reported that the midpoint potential of wild-type FMN-bp is −325 mV on a graphite electrode, but in the current system we estimated its value as −277 mV (*vs* Normal Hydrogen Electrode). The difference is probably due to a structural change of the protein upon adsorption onto the graphite electrode surface.

We further found that the midpoint potentials were affected by all of the mutations. The midpoint potential of the L122del mutant changed only slightly (+8 mV), suggesting that Leu122 does not have a strong influence on the redox potential of FMN-bp. On the other hand, compared to the wild-type, the midpoint potential of the L122K mutant was more positive (+18 mV), the L122Y mutant was slightly more negative (−9 mV) and the L122E mutant was much more negative (−38 mV). These results indicated that, although Leu122 itself may have only a slight contribution, position 122 of FMN-bp can control the redox potential; insertion of a cationic side-chain caused the midpoint potential to be high, whereas an anionic or tyrosyl side-chain caused the midpoint potential to be low.

Dissociation Constants of Apo and FMN-bound FMN-bps—We next determined the dissociation constants at 25.0°C of the FMN–apoFMN-bp complexes and investigated the effect of point mutations at Leu122 on the

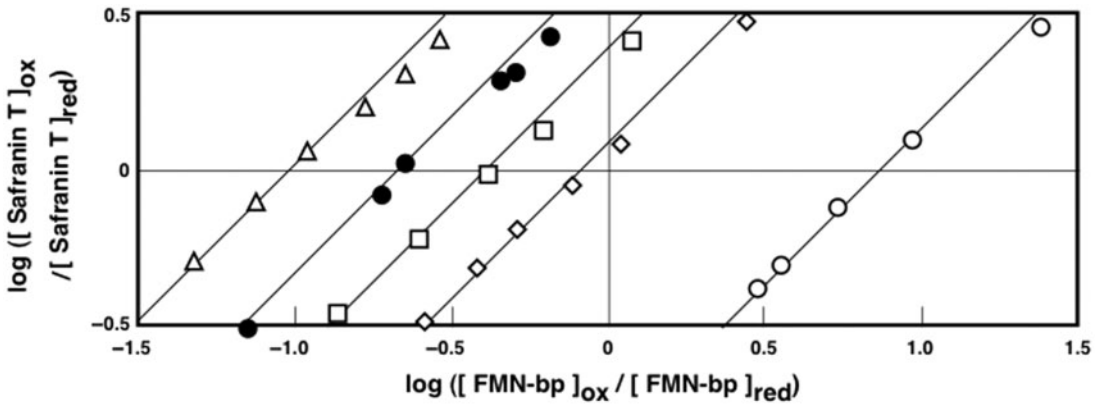

Fig. 2. **Determination of the midpoint potentials of wild-type and mutant FMN-bps.** Symbols are open triangle, L122K; closed circle, L122del; open square, wild-type; open diamond, L122Y and open circle, L122E.

Table 2. **Thermodynamic properties and solvent accessible area of a wild type and four mutants.**

Properties	Wild type	L122Y	L122E	L122K	L122del
Midpoint potential, $E_{\text{FMN-bp}}$ (mV)	−277	−286	−315	−259	−269
Dissociation constant of FMN, K_d (nM)	0.465	0.153	8.15	1.12	12.3
Free energy for the ApoFMN-bp:FMN_{ox} complex, $\triangle G_{ox}$ (kJ mol^{-1})	−53.2	−56.0	−46.1	−51.0	−45.1
Free energy for the ApoFMN-bp:FMN_{red} complex, $\triangle G_{red}$ (kJ mol^{-1})	−42.4	−43.4	−28.0	−43.7	−35.9
Dissociation constant of reduced state FMN, $K_d^{\text{reduced FMN}}$ (nM)	36.7	24.5	12,300	21.7	506
Dissociation constant of dimer, K_D (μM)	5.3	0.26	12.1	10.6	<0.26
Solvent accessible surface area (Å^2)	85	66	77	81	–

dissociation of FMN. In all cases, over most of the titration curve, the fluorescence decrease was linear with the amount of wild-type or mutant apoFMN-bp added, indicating that the complex is strong enough to allow the determination of K_d. We were able to obtain an estimate of the K_d for these complexes from only three experimental points that were close to the equivalence point and off the linear parts of the titration curve (Fig. 3). The dissociation constant between FMN and wild-type apoFMN-bp (Table 2) was nearly the same as between FMN and apoflavodoxin (*3*). The L122Y mutant apoprotein had an affinity for oxidized FMN ~3-fold higher than the wild-type apoFMN-bp, whereas the L122E, L122K and L122del mutants had lower affinities for FMN than wild-type protein (Table 2). On the other hand, the ΔG_{red} values of wild-type and mutant FMN-bps showed that for reduced FMN and apoFMN-bp, L122Y and L122K mutants had slightly higher affinities than the wild type, while L122E and L122del mutants had much lower affinities than the wild type.

Dissociation Constants for Dimer Formation by Wild-type and Mutant FMN-bps—To further examine the role of Leu122, we determined the dissociation constants of dimer formation for wild-type and mutant FMN-bps at 20.0°C (Table 2). For L122Y and L122del mutants, monomer binding was tighter than for the wild type, whereas for L122E and L122K mutants, it was weaker than for the wild-type.

X-ray Crystallography—Crystals suitable for X-ray analysis (0.1 to 0.3 mm) were obtained in 1 week by hanging drop vapour diffusion. The crystals of L122Y and L122K mutants diffracted up to 1.6 Å resolution, whereas the L122E crystal diffracted to ~1.9 Å resolution. All crystals belonged to the monoclinic space group $P2_1$. Unit cell parameters were $a = 36.67$, $b = 79.39$, $c = 39.97$ Å and $\beta = 91.25°$ for L122Y; $a = 60.16$, $b = 57.96$, $c = 62.02$ Å and $\beta = 91.54°$ for L122E; and $a = 36.72$, $b = 83.32$, $c = 40.41$ Å and $\beta = 93.86°$ for L122K. A total of 27,871 (L122Y), 32,810 (L122E) and 29,879 (L122K) unique reflections were obtained, and the overall R_{merge} was 3.2% (L122Y), 7.7% (L122E) and 2.8% (L122K) with excellent completeness (98.0 to 99.5%). The size of the unit cell of the L122K mutant was approximately the same as that of the L122Y mutant, but the unit cell for the L122E crystal was different for each axis and the volume was twice of the other two point mutants. Therefore, the L122Y and L122K crystals contained one dimer in the asymmetric unit, while the L122E crystal contained two dimers.

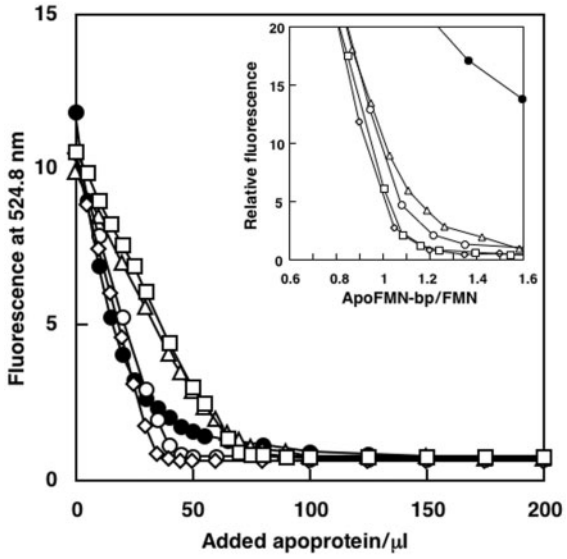

Fig. 3. **Determination of dissociation constants for the complexes of FMN with wild-type and mutant apoFMN-bps.** Symbols are open triangle, L122K; closed circle, L122del; open square, wild-type; open diamond, L122Y and open circle, L122E.

The structures for L122Y, L122E and L122K mutants were refined to a *R*-factor of 15.3% ($R_{free} = 18.5\%$) at 1.6 Å, 18.4% ($R_{free} = 21.2\%$) at 1.9 Å and 17.0% ($R_{free} = 18.8\%$) at 1.6 Å, respectively (Table 3). Other refinement statistics and the number of water molecules found in the refinement stage are summarized in Table 3. The stereochemical quality of the structures as assessed by *PROCHECK* was excellent (*31*), and the results of the Ramachandran plots are also shown in Table 3.

Crystal Structure of Mutant FMN-bps—There are two FMN-bp molecules (Monomer-A and -B) in each dimer in the asymmetric unit for L122Y (Fig. 4a) and L122K (Fig. 4b) mutants, whereas there are four FMN-bp molecules (two dimers) for the L122E mutant (Fig. 4c). The two monomers in the dimeric form are related by a non-crystallographic 2-fold axis parallel to the crystallographic *b*-axis, and the two dimers in L122E are related by translation within a plane (almost parallel to the *a*–*b* plane).

Superimposition of the monomer structures of the three mutant proteins based on core structures for α-helices (α1, 4–10; α2, 52–60; α3, 96–99) and β-strands (β1, 15–21; β2a, 26–32; β2b, 37–39; β3, 43–48; β4, 63–74; β5, 79–92; β6, 109–120) revealed that the molecular surface deviates at only several points of the turn structures (Fig. 5). Similarly, there was no apparent structural difference when the molecules in the dimeric form were superimposed. The root mean square deviation

Table 3. **Refinement statistics.**

Refinement	L122Y	L122E	L122K
Resolution (Å)[a]	1.60 (1.66–1.60)	1.90 (1.97–1.90)	1.60 (1.66–1.60)
No. of reflections	27,871	32,810	29,879
R-factor (%)[a]	15.3 (15.7)	18.4 (20.7)	17.0 (16.5)
R_{free} (%)[a]	18.5 (–)	21.2 (25.6)	18.8 (18.7)
Number of atoms			
Protein	1967	3832	1920
Solvent	440	420	275
R.m.s deviations			
Bonds (Å)	0.01	0.01	0.01
Angles (°)	0.02	1.26	1.25
Ramachandran plot (%)			
Most favoured	91.6	90.8	92.1
Additional allowed	8.4	9.2	7.9
Generously allowed	0.0	0.0	0.0
Disallowed	0.0	0.0	0.0

[a]Values in outer shell are in parentheses.

of the α-carbon atoms calculated between each set of superimposed molecules both in monomeric and dimeric forms ranges from 0.15 to 0.25 Å (Table 4). The root mean square deviation for monomers was determined by setting a larger mean temperature factor for one of the two monomers in the dimer structure (one of the four monomers for the L122E structure). The small root mean square deviations indicate that the main-chain folding pattern of the monomer molecules and the conformation of the two monomers in the dimeric structure are nearly identical.

In the crystal structure of wild-type FMN-bp, one monomer (Monomer-A) holds one cofactor FMN at the amino terminal end of the second α-helix (α2) by hydrogen bonding (Table 5). The *o*-xylene moiety is covered by the carboxyl-terminal loop of Monomer-B. As a result, FMN is situated in the groove of the dimer interface by hydrophobic and hydrophilic interactions. The structures and the scheme of hydrogen bonding interactions between amino acid side-chains of Monomer-A and FMN of each mutant protein were almost identical to those found in the structure of the wild-type molecule. The side chain of Leu122 at the carboxyl terminus of Monomer-B covered the FMN group and appears to protect FMN from the solvent. Figure 6 shows superimposed crystal structures around the FMN molecule in the mutant proteins. In the three point mutants, the tyrosine side-chain in the L122Y mutant has double conformers. The lysine side-chain in the L122K mutant is directed toward the opposite side as side chains in Tyr122, Glu122 and Leu122 mutants because of the hydrogen bonding between the Nζ atoms of Lys122 and

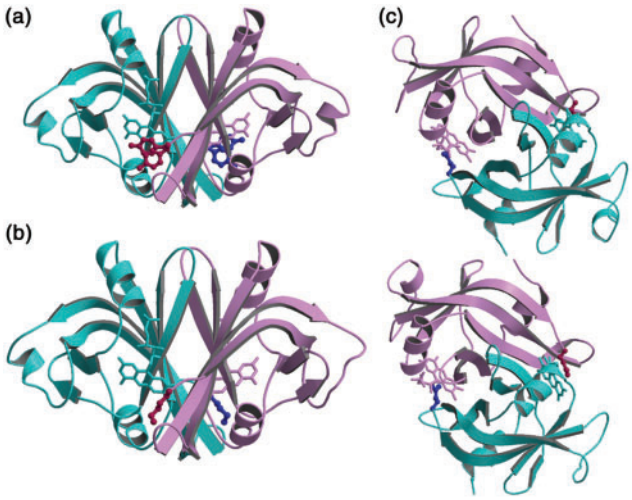

Fig. 4. **Ribbon model of two monomer molecules in an asymmetric unit of (a) L122Y (two conformers of Y122 are shown), (b) L122K and (c) Two dimers (four monomer molecules) of L122E.** Monomers are related by a non-crystallographic 2-fold axis. They are related by translation within a plane almost parallel to the *a*–*b* plane. The FMN group is shown as a stick model, whereas mutated residues (L122Y, L122K and L122E) are shown as ball-and-stick models. FMN molecules are shown in the same colour as the monomer molecule to which it belongs. Mutated residues are shown in red in the pink monomer and blue in the cyan monomer. The figures were prepared using MOSCRIPT and Raster3D (*43*, *44*).

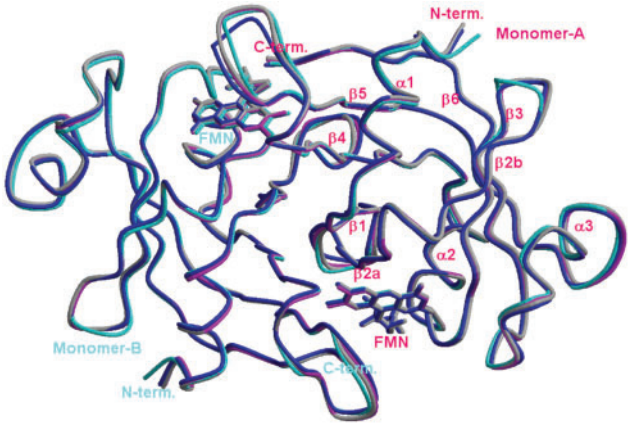

Fig. 5. **Superimposition of the wild-type and the three mutant FMN-binding protein molecules in a dimeric form.** Wild-type, L122Y, L122K and L122E molecules are shown in gray, blue, red and cyan, respectively. Typical secondary structures, α-helices (α1, 4–10; α2, 52–60 and α3, 96–99), and β-strands (β1, 15–21; β2a, 26–32; β2b, 37–39; β3, 43–48; β4, 63–74; β5, 79–92 and β6, 109–120) are labelled according to Suto *et al.* (*12*).

Table 4. **Root mean square deviations of superimposed FMN-bp molecules in monomeric and dimeric forms between intra- and inter-mutant.**

	Root mean square deviation (Å)			
	Wild type	L122Y	L122E	L122K
In monomeric form				
Wild type	0.09	–	–	
L122Y	0.19	0.19	–	–
L122E	0.28	0.34	0.20	–
L122K	0.14	0.17	0.29	0.11
In dimeric form				
L122Y	0.23	–	–	
L122E	0.21	0.22	0.19[a]	
L122K	0.16	0.16	0.19	

Note: In rmsd calculation of inter-mutants, the molecule with the larger B value in the dimer was selected.
[a]The value is calculated between two dimers in L122E.

Table 5. **Some interactions between amino acid side-chain and FMN within 4.0 Å.**

Side-chain atoms (residue)			
Wild type	L122Y	L122E	L122K
NE2 (His27)	NE2 (His27)	NE2 (His27)	NE2 (His27)
CB (Val29)	CB (Val29)	CB (Val29)	CB (Val29)
OG1 (Thr31)	OG1 (Thr31)	OG1 (Thr31)	OG1 (Thr31)
NE1 (Trp32)	NE1 (Trp32)	NE1 (Trp32)	NE1 (Trp32)
CD1 (Tyr35)	CD1 (Tyr35)	CD1 (Tyr35)	CD1 (Tyr35)
CE (Met51)	CE (Met51)	CE (Met51)	CE (Met51)
NZ (Lys53)	NZ (Lys53)	NZ (Lys53)	NZ (Lys53)
OG1 (Thr54)	OG1 (Thr54)	OG1 (Thr54)	OG1 (Thr54)
CH2 (Trp106)	CH2 (Trp106)	CH2 (Trp106)	CH2 (Trp106)
OG1 (Ser121B)	OG1 (Ser121B)	OG1 (Ser121B)	OG1 (Ser121B)
CD2 (Leu122B)	CZ (Tyr122B)	OE2 (Glu122B)	CB (Asn30)
		CG2 (Val15B)	

the carbonyl oxygen atoms of Pro79 and Gly80 of the same monomer. Based on the crystal structures, the *CNS* program calculated the solvent-accessible surface areas of the FMN group as 66, 81, 77 and 85 Å^2 for the L122Y, L122K, L122E and wild-type proteins (Table 2). The accessibility of FMN (L122Y < L122K ≈ L122E < wild-type) shows some correlation with the bulkiness (L122Y > L122E ≈ L122K > wild-type) of the side-chain group at carboxyl terminus.

DISCUSSION

As the midpoint potentials of the wild-type and the deletion mutant were only slightly different, it appears that a carboxyl-terminal leucine is not important in determining the midpoint potential; however, the midpoint potential must be effectively controlled by the amino acid at position 122, which is located near the *o*-xylene moiety of FMN, because all of the amino-acid substitutions affected the midpoint potentials. It has been reported that Glu and Asp residues, which are clustered around the FMN-binding site and within 13 Å of the N(1) atom of FMN, have electrostatic effects on the redox potential (*19*). Moreover, in the case of the T56G mutant of flavodoxin from *Anabaena*, it was shown that the increased accessibility of FMN led to an increase of +63 mV in the $E_{sq/red}$ value and a correlation between the electrostatic environment of FMN and the $E_{sq/red}$ value has been observed. The more positive the residues or the less negative the residues present in the surroundings of the FMN N(1) atom, the less negative the value of $E_{sq/red}$ (*32*). Similar electrostatic effects must occur in the L122E mutant, and opposite effects may occur in the L122K mutant. The L122Y mutant showed a slightly negative change in the midpoint potential, which likely represents the average of the conformer values. This change may have been caused by some other interactions, for example, another hydrophobic interaction between the *o*-xylene moiety of FMN and the aromatic moiety of the tyrosine residue. Indeed, the apo-L122Y mutant had a higher affinity for FMN than the wild-type protein, and the dissociation constant of dimer formation for the L122Y mutant was smaller than for the wild-type protein. These results support the existence of a hydrophobic interaction between the *o*-xylene moiety of FMN and the aromatic moiety of the tyrosine residue. In addition, it appears that the hydrogen-bonding network is conserved because the water molecules were in similar positions in the mutant and wild-type FMN-bps (Fig. 6).

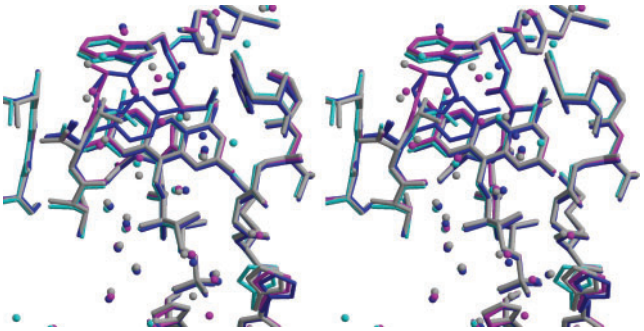

Fig. 6. **Stereo drawing of the stick model around the FMN of each molecule.** The wild-type and three mutant molecules are superimposed and coloured as in Fig. 4. Two conformers of the side chain of Tyr122 are shown for the L122Y mutant. Balls represent water molecules.

On the other hand, the dissociation constants of the complexes between oxidized FMN and mutant apoL122E, apoL122K and apoL122del were larger than that of the wild-type protein (L122del > L122E > L122K > wild-type > L122Y). Although the accessibility of FMN shows some correlation with the bulkiness of the side-chain group at the carboxyl-terminal end, the bulkiness of the side-chain group and solvent accessibility do not appear to be related to the dissociation constant of FMN. It seems that the dissociation of FMN depends on not only the bulkiness, but also the hydrophobicity of the side-chain of the residue at the carboxyl-terminus; in other words, the hydrophobic interaction between Leu122 in the pairing molecule and FMN was important for the binding of FMN. While in most flavodoxins the FMN is stacked against a Tyr residue on its *si* face and a Trp residue on its *re* face, in the case of flavodoxin II from *Azotobacter vinelandii*, Leu57 was positioned at the *re* face of FMN and was thought to contribute to the more polar FMN-binding site and stabilized the hydroquinone form. In this case, two water molecules were situated to fill up an open cavity created by a smaller Leu residue at the *re* face of FMN (*33*); however, FMN-bp showed a different structure, that is, the crystal structure of wild-type and mutant FMN-bps showed no water molecule between the FMN and Leu122 residue. Although the calculated dissociation constants for reduced FMN were larger than those for oxidized FMN in all cases, the K_d values of the complexes between reduced FMN and apoL122E and apoL122del mutants were much larger than that of wild-type protein while those of apoL122Y and apoL122K were slight smaller than that of wild-type protein. This might have been caused by the hyroquinone repulsing the side chain of the Glu residue while the hydroquinone interacted with the side chain of Tyr and Lys in L122Y and L122K. The unstable FMN molecule in L122del may be due to a lack of sufficient space in the FMN-binding pocket because the interactions between monomers are too tight. It is said the hydrogen-bonding network in the FMN environment influences FMN affinity (*32*), such network and water molecules in all mutants seem to be conserved and no discussion is needed in this study. In the case of L122E, the mutation caused the side-chain of His52 to be positioned close to the phosphate group of FMN, whereas in other mutants, it was moved away from the phosphate group of FMN (Fig. 6). It seems that there is some interaction between the side-chain of His52 and the phosphate group of FMN, but there is no obvious correlation between the distances and dissociation constants for the formation of the FMN–apoprotein complex. For flavodoxin, there are only a few hydrogen bonds between the phosphate group of FMN, the amide groups of Thr11, Thr12, Asn14 and Thr15 and the hydroxyl groups of Ser10, Thr11, Thr15 and Ser58, and there is no basic amino-acid residue near the phosphate group of FMN (*34*).

The values of the dissociation constants for dimers (L122E > L122K > wild-type > L122Y > L122del) show that

a larger volume of the hydrophobic unit of the side-chain group at the carboxyl-terminal end has a tendency to contribute to tighter interactions between two monomers in a dimer. This may be another reason why the interaction between FMN and the hydrophilic functional group of Glu ($-COO^-$) or Lys ($-NH_3^+$) residues are weaker than between FMN and the hydrophobic Leu residue. Importantly, L122del has the smallest dissociation constant among the mutants tested. This may have been due to a reduction in the distance between pairing monomers, which in turn would have increased the other inter-monomer interactions. This also suggests that the carboxyl-terminal residue helps prevent monomers from interacting too tightly so that they can dissociate when the monomeric form is required. In fact, even though we screened multiple conditions, we were unable to crystallize the L122del mutant. The importance of dimerization was discussed in the transcription factor fumarate nitrate reduction, a major O_2 sensor (*35*). The cofactor, oxygen labile [4Fe–4S] cluster, was required for dimerization and was essential for activity. In the case of FMN-bp, the significance of dimerization is still not clear, but our recent data clarified that even apoFMN-bp can form mainly dimers using an apoFMN-bp expressed wheat germ cell-free protein synthesis system (*36*).

Similar studies that clarified the importance of carboxyl-terminal amino-acid residue have been performed on monomer enzyme, pea and *Anabaena* ferredoxin-$NADP^+$ reductase. The carboxyl-terminal Tyr residue, forming a stacking interaction with the isoalloxazine ring of FAD, plays roles not only in modulating flavin redox properties (*37*), but also in nicotinamide binding and hydride transfer (*38*). Although the carboxyl-terminal residue is important in both ferredoxin-$NADP^+$ reductase and FMN-bp, there is quite a difference in activity. In fact, the midpoint potentials must be effectively controlled by amino acid at position 122 in the FMN-bp; however, a carboxyl-terminal Leu residue is not important in determining the midpoint potential from the results of L122del mutant.

Recently, the genome sequence of *D. vulgaris* Hildenborough was determined (*39*). This is a different strain of *D. vulgaris* used in this study, and its genome lacks a homologue of FMN-bp. In contrast, some other bacteria (*Clostridium acetobutylicum*, *Streptococcus agalactiae* NEM316 and *Lactococcus lactis* subsp. *Lactis*) have a gene homologous to FMN-bp. This suggests that FMN-bp may function under anaerobic conditions but that it may not be an essential protein; however, the three-dimensional structure of FMN-bp is similar to that of pyridoxine 5′-phosphate oxidase (PNPOx) from *E. coli*, although their amino-acid sequences are unrelated (*40*). PNPOx catalyses the synthesis of pyridoxal 5′-phosphate and hydrogen peroxide (or ammonium) from oxygen and pyridoxine 5′-phosphate (or pyridoxamine 5′-phosphate). We were unable to detect this activity (*41*) in FMN-bp (data not shown), which is not surprising because this reaction utilizes oxygen as a substrate and *D. vulgaris* is an obligate anaerobe. If FMN-bp catalyses this reaction, some other substrate must be used instead of oxygen. Indeed, the *D. vulgaris* Hildenborough genome lacks the gene for PNPOx (*pdxH*), and its amino-acid sequence is highly conserved; however, it does contain *pdxA* and *pdxJ* homologues, which are thought to catalyse reactions in the vitamin B_6 biosynthesis pathway. Recently, the overall fold of conserved hypothetical protein Rv1155 *from Mycobacterium tuberculosis* was found to resemble that of FMN-bp and PNPOx; however, it is not able to bind even FMN (*42*); therefore, because the physiological function of FMN-bp remains unclear, we cannot discuss the relationship between its physiological function *in vivo* and either the redox properties, FMN-binding properties, or dimer formation.

The atomic coordinates of the three mutant FMN-binding proteins have been deposited in the Protein Data Bank under ID numbers 1WLI (L122Y), 1WLK (L122E) and 1WLL (L122K). We thank Dr K. Yutani and Ms M. Sakai of the Institute of Protein Science, Osaka University for analytical ultracentrifugation. This work was partly supported by a Grant-in-Aid to M.K. for the Encouragement of Young Scientists from the Ministry of Education, Science, Sports and Culture of Japan and by grants to Y.H. from the 21st Century COE and the National Project on Protein Structural and Functional Analyses of Japan.

REFERENCES

1. Ulmer, K.M. (1983) Protein engineering. *Science* **219**, 666–671
2. Chen, L., Liu, M.-Y., and LeGall, J. (1995) Characterization of electron transfer proteins. in *Sulfate-Reducing Bacteria* (Barton, L.L., ed.) pp. 113–149, Plenum Press, New York
3. Kitamura, M., Sagara, T., Taniguchi, M., Ashida, M., Ezoe, K., Kohno, K., Kojima, S., Ozawa, K., Akutsu, H., Kumagai, I., and Nakaya, T. (1998) Cloning and expression of the gene encoding flavodoxin from *Desulfovibrio vulgaris* (Miyazaki F). *J. Biochem.* **123**, 891–898
4. Kitamura, M., Kojima, S., Ogasawara, K., Nakaya, T., Sagara, T., Niki, K., Miura, K., Akutsu, H., and Kumagai, I. (1994) Novel FMN-binding protein from *Desulfovibrio vulgaris* (Miyazaki F) -Cloning and expression of its gene in *Escherichia coli*. *J. Biol. Chem.* **269**, 5566–5573
5. Agostinho, M., Oliveira, S., Broco, M., Liu, M.–Y., LeGall, J., and Rodrigues-Pousada, C. (2000) Molecular cloning of the gene encoding flavoredoxin, a flavoprotein from *Desulfovibrio gigas*. *Biochem. Biophys. Res. Commun.* **272**, 653–656
6. Chen, L., Liu, M.–Y., LeGall, J., Fareleira, P., Santos, H., and Xavier, A.V. (1993) Purification and characterization of an NADH-rubredoxin oxidoreductase involved in the utilization of oxygen by *Desulfovibrio gigas*. *Eur. J. Biochem.* **216**, 443–448
7. Peck, H.D.Jr, Deacon, T.E., and Davidson, J.T. (1965) Studies on adenosine 5′-phosphosulfate reductase from *Desulfovibrio desulfuricans* and *Thiobacillus thioparus*. I. The assay and purification. *Biochim. Biophys. Acta* **96**, 429–446
8. Swenson, R.P. and Krey, G.D. (1994) Site-directed mutagenesis of tyrosine-98 in the flavodoxin from *Desulfovibrio vulgaris* (Hildenborough): regulation of oxidation-reduction properties of the bound FMN cofactor by aromatic, solvent, and electrostatic interactions. *Biochemistry* **33**, 8505–8514
9. Liepinsh, E., Kitamura, M., Murakami, T., Nakaya, T., and Otting, G. (1997) Pathway of chymotrypsin evolution suggested by the structure of the FMN-binding protein from *Desulfovibrio vulgaris* (Miyazaki F). *Nature Struct. Biol.* **4**, 975–979

10. Murzin, A.G. (1998) Probable circular permutation in the flavin-binding domain. *Nature Struct. Biol.* **5**, 101
11. Liepinsh, E., Kitamura, M., Murakami, T., Nakaya, T., and Otting, G. (1998) Common ancestor of serine proteases and flavin-binding domains. *Nature Struct. Biol.* **5**, 102–103
12. Suto, K., Kawagoe, K., Shibata, N., Morimoto, Y., Kitamura, M., Nakaya, T., and Yasuoka, N. (1999) Crystallization and preliminary crystallographic studies of FMN-binding protein from *Desulfovibrio vulgaris* Miyazaki F. *Acta Crystallogr.* **D55**, 1089–1090
13. Suto, K., Kawagoe, K., Shibata, N., Morimoto, Y., Higuchi, Y., Kitamura, M., Nakaya, T., and Yasuoka, N. (2000) How do the X-ray structure and the NMR structure of FMN-binding protein differ? *Acta Crystallogr.* **D56**, 368–371
14. Watenpaugh, K.D., Sieker, L.C., Jensen, L.H., LeGall, J., and Dubourdieu, M. (1972) Structure of the oxidized form of a flavodoxin at 2.5-Å resolution: resolution of the phase ambiguity by anomalous scattering. *Proc. Natl. Acad. Sci. USA.* **69**, 3185–3188
15. Stockman, B.J., Richardson, T.E., and Swenson, R.P. (1994) Structural changes caused by site-directed mutagenesis of tyrosine-98 in *Desulfovibrio vulgaris* flavodoxin delineated by ^{1}H and ^{15}N NMR spectroscopy: implications for redox potential modulation. *Biochemistry* **33**, 15298–15308
16. Murray, T.A. and Swenson, R.P. (2003) Mechanism of flavin mononucleotide cofactor binding to the *Desulfovibrio vulgaris* flavodoxin. 1. Kinetic evidence for cooperative effects associated with the binding of inorganic phosphate and the 5'-phosphate moiety of the cofactor. *Biochemistry* **42**, 2307–2316
17. Curley, G.P., Carr, M.C., Mayhew, S.G., and Voordouw, G. (1991) Redox and flavin-binding properties of recombinant flavodoxin from *Desulfovibrio vulgaris* (Hildenborough). *Eur. J. Biochem.* **202**, 1091–1100
18. Murray, T.A., Foster, M.P., and Swenson, R.P. (2003) Mechanism of flavin mononucleotide cofactor binding to the *Desulfovibrio vulgaris* flavodoxin. 2. Evidence for cooperative conformational changes involving tryptophan 60 in the interaction between the phosphate- and ring-binding subsites. *Biochemistry* **42**, 2317–2327
19. Zhou, Z. and Swenson, R.P. (1995) Electrostatic effects of surface acidic amino acid residues on the oxidation-reduction potentials of the flavodoxin from *Desulfovibrio vulgaris* (Hildenborough). *Biochemistry* **34**, 3183–3192
20. Bradley, L.H. and Swenson, R.P. (2001) Role of hydrogen bonding interactions to N(3)H of the flavin mononucleotide cofactor in the modulation of the redox potentials of the *Clostridium beijerinckii* flavodoxin. *Biochemistry* **40**, 8686–8695
21. McCarthy, A.A., Walsh, M.A., Verma, C.S., O'Connell, D.P., Reinhold, M., Yalloway, G.N., D'Arcy, D., Higgins, T.M., Voordouw, G., and Mayhew, S.G. (2002) Crystallographic investigation of the role of aspartate 95 in the modulation of the redox potentials of *Desulfovibrio vulgaris* flavodoxin. *Biochemistry* **41**, 10950–10962
22. Kumagai, I., Kojima, S., Tamaki, E., and Miura, K. (1987) Conversion of Trp62 of hen egg-white lysozyme to Tyr by site-directed mutagenesis. *J. Biochem.* **102**, 733–740
23. Laemmli, U.K. (1970) Cleavage of structural proteins during the assembly of the head of bacteriophage T4. *Nature* **227**, 680–685
24. Lambeth, J.D. and Kamin, H. (1976) Adrenodoxin reductase. Properties of the complexes of reduced enzyme with $NADP^{+}$ and NADPH. *J. Biol. Chem.* **251**, 4299–4306
25. Alberty, R.A. (1998) Calculation of standard transformed formation properties of biochemical reactants and standard apparent reduction potentials of half reactions. *Arch. Biochem. Biophys.* **358**, 25–39
26. Laue, T.M. and Stafford, W.F.3rd. (1999) Modern applications of analytical ultracentrifugation. *Annu. Rev. Biophys. Biomol. Struct.* **28**, 75–100
27. Otwinowski, Z. and Minor, W. (1997) Processing of X-ray diffraction data collected in oscillation mode. *Methods Enzymol.* **276**, 307–326
28. Perrakis, A., Morris, R., and Lamzin, V.S. (1999) Automated protein model building combined with iterative structure refinement. *Nature Struct. Biol.* **6**, 458–463
29. Brünger, A.T., Adams, P.D., Clore, G.M., DeLano, W.L., Gros, P., Grosse-Kunstleve, R.W., Jiang, J.S., Kuszewski, J., Nilges, M., Pannu, N.S., Read, R.J., Rice, L.M., Simonson, T., and Warren, G.L. (1998) Crystallography & NMR system: a new software suite for macromolecular structure determination. *Acta Crystallogr.* **D54**, 905–921
30. Sheldrick, G.M. and Schneider, T.R. (1997) SHELXL: High-resolution refinement. *Methods Enzymol.* **277**, 319–343
31. Laskowski, R.A., MacArthur, M.W., Moss, D.S., and Thornton, J.M. (1993) PROCHECK: a program to check the stereochemical quality of protein structures. *J. Appl. Cryst.* **26**, 283–291
32. Nogués, I., Campos, L.A., Sancho, J., Gómez-Moreno, C., Mayhew, S.G., and Medina, M. (2004) Role of neighboring FMN side chains in the modulation of flavin reduction potentials and in the energetics of the FMN:apoprotein interaction in *Anabaena* Flavodoxin. *Biochemistry* **43**, 15111–15121
33. Alagaratnam, S., van Pouderoyen, G., Pijning, T., Dijkstra, B.W., Cavazzini, D., Rossi, G.L., Van Dongen, W.M., van Mierlo, C.P., van Berkel, W.J., and Canters, G.W. (2005) A crystallographic study of Cys69Ala flavodoxin II from *Azotobacter vinelandii*: structural determinants of redox potential. *Protein Sci.* **14**, 2284–2295
34. Walsh, M.A., McCarthy, A., O'Farrell, P.A., McArdle, P., Cunningham, P.D., Mayhew, S.G., and Higgins, T.M. (1998) X-ray crystal structure of the *Desulfovibrio vulgaris* (Hildenborough) apoflavodoxin-riboflavin complex. *Eur. J. Biochem.* **258**, 362–371
35. Moore, L.J., Mettert, E.L., and Kiley, P.J. (2006) Regulation of FNR dimerization by subunit charge repulsion. *J. Biol. Chem.* **281**, 33268–33275
36. Abe, M., Ohno, S., Yokogawa, T., Nakanishi, T., Arisaka, F., Hosoya, T., Hiramatsu, T., Suzuki, M., Ogasawara, T., Sawasaki, T., Nishikawa, K., Kitamura, M., Hori, H., and Endo, Y. (2007) Detection of structural changes in a cofactor binding protein by using a wheat germ cell-free protein synthesis system coupled with unnatural amino acid probing. *Proteins*. **67**, (in press).
37. Nogués, I., Tejero, J., Hurley, J.K., Paladini, D., Frago, S., Tollin, G., Mayhew, S.G., Gomez-Moreno, C., Ceccarelli, E.A., Carrillo, N., and Medina, M. (2004) Role of the C-terminal tyrosine of ferredoxin-nicotinamide adenine dinucleotide phosphate reductase in the electron transfer processes with its protein partners ferredoxin and flavodoxin. *Biochemistry* **43**, 6127–6137
38. Tejero, J., Pérez-Dorado, I., Maya, C., Martínez-Júlvez, M., Sanz-Aparicio, J., Gómez-Moreno, C., Hermoso, J.A., and Medina, M. (2005) C-terminal tyrosine of ferredoxin-$NADP^{+}$ reductase in hydride transfer processes with $NAD(P)^{+}$/H. *Biochemistry* **44**, 13477–13490
39. Heidelberg, J.F., Seshadri, R., Haveman, S.A., Hemme, C.L., Paulsen, I.T., Kolonay, J.F., Eisen, J.A., Ward, N., Methe, B., Brinkac, L.M., Daugherty, S.C., Deboy, R.T., Dodson, R.J., Durkin, A.S., Madupu, R., Nelson, W.C., Sullivan, S.A., Fouts, D., Haft, D.H., Selengut, J., Peterson, J.D., Davidsen, T.M., Zafar, N., Zhou, L., Radune, D., Dimitrov, G., Hance, M., Tran, K., Khouri, H., Gill, J., Utterback, T.R., Feldblyum, T.V., Wall, J.D., Voordouw, G., and Fraser, C.M. (2004) The genome sequence of the anaerobic, sulfate-reducing

bacterium *Desulfovibrio vulgaris* Hildenborough. *Nature Biotech.* **22**, 554–559
40. Safo, M.K., Mathews, I., Musayev, F.N., di Salvo, M.L., Thiel, D.J., Abraham, D.J., and Schirch, V. (2000) X-ray structure of *Escherichia coli* pyridoxine 5'-phosphate oxidase complexed with FMN at 1.8 Å resolution. *Struct. Fold. Des.* **8**, 751–762
41. Zhao, G. and Winkler, M.E. (1995) Kinetic limitation and cellular amount of pyridoxine (pyridoxamine) 5'-phosphate oxidase of *Escherichia coli* K-12. *J. Bacteriol.* **177**, 883–891
42. Canaan, S., Sulzenbacher, G., Roig-Zamboni, V., Scappuccini-Calvo, L., Frassinetti, F., Maurin, D., Cambillau, C., and Bourne, Y. (2005) Crystal structure of the conserved hypothetical protein Rv1155 from *Mycobacterium tuberculosis*. *FEBS Lett.* **579**, 215–221
43. Kraulis, P.K. (1991) MOLSCRIPT: a program to produce both detailed and schematic plots of protein structures. *J. Appl. Crystallogr.* **24**, 946–950
44. Merritt, E.A. and Murphy, M.E. (1994) Raster3D Version 2.0. A program for photorealistic molecular graphics. *Acta Crystallogr.* **D50**, 869–873